



Master of Mechanical and Aerospace of Engineering

**POTENTIAL FLOWS ABOUT
AIRFOILS/HYDROFOILS WITH ONE- AND TWO-
WAY COUPLED BOUNDARY LAYER MODELS**

Report on Thesis Project

By

Yerkegali Metey

Principal Supervisor: Konstantinos Kostas

December, 2018

DECLARATION

I hereby, declare that this manuscript, entitled “Potential Flows about Airfoils/Hydrofoils with One- and Two-Way Coupled Boundary Layer Models”, is the result of my own work except for quotations and citations which have been duly acknowledged.

I also declare that, to the best of my knowledge and belief, it has not been previously or concurrently submitted, in whole or in part, for any other degree or diploma at Nazarbayev University or any other national or international institution.

Name: Yerkegali Metey
Date: 13.12.2018

Potential Flows about Airfoils/Hydrofoils with One- and Two-Way Coupled Boundary Layer Models

Yerkegali Metey

Nazarbayev University, Astana, Kazakhstan

ABSTRACT

The main objectives of this thesis are to implement the one- and two-way couplings of an inviscid flow formulation with an appropriate boundary layer model and to verify and benchmark the implementations against experimental results. The coupling between the boundary layer and the inviscid formulation allows a quick calculation of the most important aerodynamic/hydrodynamic coefficients, i.e., lift and drag coefficients. There are two possibilities when coupling inviscid formulations with boundary layer models: one- and two-way couplings. One-way coupling model neglects the effect of the boundary layer thickness on the body itself, i.e., the modification of the shape that the flow sees. In one-way coupling, the initial tangential velocity distribution along the body coming from the inviscid model is used for the computation of the boundary layer and subsequently the calculation of drag. In two-way coupling, the boundary layer thickness, which is computed in the boundary layer model, modifies the shape of the airfoil used in the inviscid model and a second computation of the tangential velocities around the modified body is performed. The procedure is repeated till we achieve the required convergence. Obviously, two-way coupling is generally expected to produce more accurate results.

ACKNOWLEDGMENTS

First, I would like to express my gratitude towards my advisor Professor Konstantinos Kostas for the continuous support of my graduate study and research, for his patience, motivation, and provided opportunities. Moreover, I would like to thank the thesis committee, Professors of Mechanical and Aerospace Engineering Department for their support and contribution.

TABLE OF CONTENTS

ABSTRACT.....	ii
LIST OF FIGURES.....	iv
LIST OF TABLES.....	v
LIST OF ABBREVIATIONS, NOTATIONS / GLOSSARY OF TERMS.....	vi
1. INTRODUCTION.....	1-2
2. LITERATURE REVIEW.....	3
2.1. Introduction to Fluid Mechanics.....	3-4
2.1.1. Compressible and Incompressible flow.....	4-5
2.1.2. Fluid Flow Analysis.....	5-6
2.1.3. Laminar and Turbulent Flow.....	6-7
2.1.4. Bernoulli's Equation.....	7
2.2. Aerodynamics.....	8-11
2.3. Boundary Layers.....	11-14
2.4. Present Research Objectives.....	15
3. METHODOLOGY.....	16
3.1. The Inviscid Flow model.....	16-17
3.2. Pablo.....	17
3.2.1. Thwaites' Model.....	18-19
3.2.2. Head's Model.....	19-20
3.2.3. Michel's Criterion	21-22
3.3. IGA-BEM Solver.....	22
3.3.1. Governing equations.....	22-27
3.4. Xfoil.....	27-30
4. RESULTS AND DISCUSSION.....	31
4.1. Results of Inviscid Flow Model in Pablo and IGA.....	31-40
4.2. Results of Viscous Flow Model in Xfoil.....	41-43
5. CONCLUSION.....	44
REFERENCES.....	45-46
APPENDICES.....	47-49

LIST OF FIGURES

Figure 2.2.1: Airfoil

Figure 2.3.1: Development of the boundary layer

Figure 2.3.2: Development of a wake region

Figure 3.3.1.1: A hydrofoil in a flow with velocity \vec{U}_∞ and its wake boundary $\partial\Omega_w$

Figure 3.4.1. Xfoil interface

Figure 3.4.2: Set up procedure for the (a) original xfoil; (b) adapted xfoil viscous formulation

Figure 4.1.1: C_l against number of panels and DOF of an NACA 4412 airfoil for 1° angle of attack (Pablo and IGA-BEM)

Figure 4.1.2: C_d against number of panels and DOF of an NACA 4412 airfoil for 1° angle of attack (PABLO and IGA-BEM)

Figure 4.1.3: C_l against number of panels and DOF of an NACA 4412 airfoil for 3° angle of attack (Pablo and IGA-BEM)

Figure 4.1.4: C_d against number of panels and DOF of an NACA 4412 airfoil for 3° angle of attack (Pablo and IGA-BEM)

Figure 4.1.5: C_l against number of panels and DOF of an NACA 4412 airfoil for 5° angle of attack (Pablo and IGA-BEM)

Figure 4.1.6: C_d against number of panels and DOF of an NACA 4412 airfoil for 5° angle of attack (Pablo and IGA-BEM)

Figure 4.1.7: C_l against number of panels and DOF of an NACA 4412 airfoil for 7° angle of attack (Pablo and IGA-BEM)

Figure 4.1.8: C_d against number of panels and DOF of an NACA 4412 airfoil for 7° angle of attack (Pablo and IGA-BEM)

Figure 4.2.1. Original Xfoil plot

Figure 4.2.2. C_l against number of points of an NACA 4412 airfoil for 1° angle of attack

Figure 4.2.3. C_d against number of points of an NACA 4412 airfoil for 1° angle of attack

LIST OF TABLES

Table 4.1.1. Results for C_l and C_d for 1° angle of attack (Pablo and IGA)

Table 4.1.2. Results for C_l and C_d for 3° angle of attack (Pablo and IGA)

Table 4.1.3. Results for C_l and C_d for 5° angle of attack (Pablo and IGA)

Table 4.1.4. Results for C_l and C_d for 7° angle of attack (Pablo and IGA)

Table 4.2.1: Results of C_l for 1° angle of attack

Table 4.2.2: Results of C_d for 1° angle of attack

LIST OF ABBREVIATIONS, NOTATIONS / GLOSSARY OF TERMS

<i>BVP</i>	Boundary-value problem
<i>C_p</i>	pressure coefficient
<i>c</i>	speed of sound
<i>C_d</i>	drag coefficient
<i>C_l</i>	lift coefficient
<i>L</i>	lower surface
<i>M</i>	Mach number
<i>max</i>	maximum (subscript)
<i>Re</i>	Reynolds number based on free-stream conditions and airfoil chord
<i>S</i>	boundary-layer separation location
<i>T</i>	transition (subscript)
<i>U</i>	upper surface
<i>X</i>	airfoil abscissa
<i>z</i>	airfoil ordinate
<i>α</i>	angle of attack relative to x-axis
<i>H</i>	shape factor
<i>C_f</i>	skin friction coefficient
<i>h</i>	height of the fluid
<i>ρ</i>	density of the fluid
<i>g</i>	acceleration due to gravity
<i>∂Ω_B</i>	boundary layer thickness

1. INTRODUCTION

In fluid dynamics, potential flow depicts the velocity field as the scope of a scalar function, which is the velocity potential. Accordingly, irrotational velocity field defines the potential flow. The irrotational nature of a potential flow is by cause of the gradient curl of a scalar always being equivalent to zero, as the fluid particles' angular velocity is zero. The utilization area of potential flow approximation is limited. For incompressible flow, the potential theory works as the velocity potential corresponds to Laplace's equation. However, the approximation also has been utilized to depict compressible flow. Moreover, the potential flow method is used for both stationary and non-stationary flows. Applications of potential flow approximation occur, for example, in outer field flow of airfoils, water waves, groundwater flow and so on. When considering flows with strong vorticity effects, the approximation does not work. In this context, the study of the potential flows about airfoils/hydrofoils with boundary layer model is one of the main objectives of this thesis project.

In fluid mechanics, the consideration of the boundary layer is significant feature, which is the layer of the fluid close to the boundary of the body. For instance, the boundary layer around an airplane's wing

can be characterized as a thin section of flow covering the bounding surface of the wing, where viscous forces misrepresent the environing non-viscous flow. The effect of viscosity is an essential property that needs to be analyzed in the investigation of boundary layer.

The present study focuses on the potential flow around airfoils/hydrofoils with boundary layer model, based on the analysis of performance characteristics. They are lift and drag coefficients, C_l and C_d respectively, which represent the aerodynamic forces of the body immersed in the flow. The analysis of potential flow was mostly performed considering an airfoil from the NACA library, that is NACA airfoil with serial number of 4412. The shape of the airfoil is expressed as point coordinates in txt format file or directly was taken from the library of the traditional panel tools.

The ultimate objective of this thesis is to compare one-way and two-way couplings of inviscid and boundary layer models used in classical panel tools such as Pablo, Xfoil with the results coming from an IsoGeometric Analysis enabled Boundary Element (IGA-BEM) Method [4] coupled with the same Boundary Layer models.

2. LITERATURE REVIEW

2.1. Introduction to Fluid Mechanic

Fluid mechanics is the part of physics related to the mechanics of liquids, plasmas, gases and force applied to them. It has applications in an extensive variety of disciplines, such as civil, mechanical, chemical, astrophysics, geophysics, and biology. It typically divides into four main parts, which are the study of fluids at rest, fluid statics, the study of the influence of forces on fluid motion, and fluid dynamics. Fluid mechanics is considered a mathematically complex research field. There are still remains many problems, which have not been solved yet. Moreover, many problems could be only solved by using computers. This approach is called computational fluid dynamics (CFD).

Fluid dynamics is a branch of fluid mechanics, which investigates fluid flow. It is also referred to as the science of gases and fluids in motion. Fluid mechanics presents an efficient structure that covers semi-empirical and empirical laws obtained from flow measurement and utilized for real practical issues. A typical problem in fluid dynamics involves deriving several properties, such as pressure, temperature, velocity, and density, as functions of time and space. Fluid dynamics is also divided into several branches, such as aerodynamics and

hydrodynamics. Aerodynamics is the research of air and gases in motion, while hydrodynamics is the research of liquids in motion. The application of fluid dynamics can include calculating the mass flow rate of liquid in pipelines, determining forces and movements on a plane, forecasting developing weather patterns, modeling explosions, and observing nebulae in space. Moreover, crowd dynamics and traffic engineering utilize some principles of fluid dynamics.

2.1.1. Compressible and Incompressible flow

The fluid flow is considered as incompressible flow when the density (ρ) of the fluid is constant. More specifically, it is true, if the density is not changed through its travel in a particular field. In reality, however, fluids of all type are regarded as compressible. However, for fluids with a low factor of compressibility and/or when the density, ρ , is constant within a small element volume, dV , which moves at the flow velocity U , we may assume the flow to be incompressible, i.e., the material derivative of the density vanishes. When considering fluid flows, one must be aware of the impacts of compressibility and must make sure that the aforementioned condition holds when considering incompressible flow formulations. Nonetheless, when considering

gasses, compressibility turns into a noteworthy issue and it is most imperative when the speed of the flow comes close to the speed of sound of the fluid [11]. For instance, the speed of sound in air is about 343m/s ($T = 20^{\circ}C$) while dealing with air. Thus, compressibility impacts must be considered when the ratio of the speed flow to the speed of sound exceeds 30%. This ratio is named Mach Number and is used as a criterion for this consideration [11].

$$Ma = V/c \quad \text{eq. 2.1}$$

where Ma is the Mach Number, V is the velocity of the flow and c is the speed of sound. The issue of flow compressibility is raised within the generally accepted boundary limit when $Ma < 0.3$ [11]. Within the framework of this research, all airflows can be classified as incompressible because the maximum velocities obtained by the airflow were 30 m/s, which produce a maximum Mach Number of only 0.087.

2.1.2. Fluid Flow Analysis

One of the main difficulties encountered when dealing with fluid flows is that most problems are associated with an unbounded fluid domain, such as airflow through an airplane wing. So, a decision must be made regarding the boundaries of the system to be studied.

Furthermore, there are two main alternatives to studying fluid motion: firstly, a closed system which is the study of the behavior of a particular fluid element with a fixed mass; secondly, an open system, which defines a system that must be investigated as a stated area in space, or with respect to some reference system, which is control volume, through which the fluid flows. The control surface is the boundary of the system, which does not modify regarding time [3].

2.1.3. Laminar and Turbulent Flow

In 1883 Osborne Reynolds carried out an analysis in which water was discharged from a reservoir through a glass tube and a dye was introduced into the flow [3]. In accordance with this experiment, there are two completely different types of fluid flow. On one hand, it was demonstrated that the colored flow remained distinct along the entire length of the tube, indicating that a particle of water moves in parallel lines. This type of flow is known as laminar, where fluid particles move in an orderly manner and retain similar relative positions in consecutive cross-sections. On the other hand, when the speed in the tube was increased, the colored flow started to mix with the remaining flow and dissipate over the entire profile. This process is stated as turbulent flow.

The turbulent flow is characterized by chaotic changes in pressure and flow velocity [3].

2.1.4. Bernoulli's Equation

A significant attention for the development of theoretical fluid dynamics was paid by Bernoulli and Euler in the early of eighteenth century [12]. Bernoulli stated the principle combining pressure decrease with increasing flow speed, but it was Euler that derived the Bernoulli equation in its commonly found form:

$$p + \frac{1}{2}\rho V^2 + \rho gh = \text{constant} \quad \text{eq. 2.2}$$

Where p is pressure, ρ is the density of the fluid, V is the fluid flow speed, g is the gravity acceleration, h is the liquid's height. According to the developed equation, any two points along the fluid flow relate to each other in a way as represented in equation 2.3 below:

$$P_1 + \frac{1}{2}\rho V_1^2 = P_2 + \frac{1}{2}\rho V_2^2 \quad \text{eq. 2.3}$$

This is the momentum equation and is connected to the Bernoulli Equation, which basically connects pressure at any point in flow with velocity.

2.2. Aerodynamics

Aerodynamics is a branch of science that typically investigate the behavior of air movement around a solid object. The establishment of this discipline was started from initial tries of mankind to construct airplanes. The gas and fluid dynamics are used as a fundamental theory for aerodynamics. Therefore, it is considered a subcategory of mentioned disciplines with the distinction that aerodynamics mostly deals with air motion. In spite of fact that the formal establishment of discipline is the eighteenth century, the essential ideas, for example, aerodynamic drag, had been found and investigated earlier. One of the first experiments in this discipline was conducted by Wilbur and Orville Wright in 1903. The main objective of researchers was to develop airplanes. From that point forward, aerodynamics has been continually evolving with the help of wind tunnel experimentations, mathematical analysis, and computer-based simulations. Currently, it is centered on the investigation of progressively modern concepts, for example, boundary layers, supersonic and subsonic flow, compressible flow, and turbulence. Moreover, it has turned out to be progressively computational in nature.

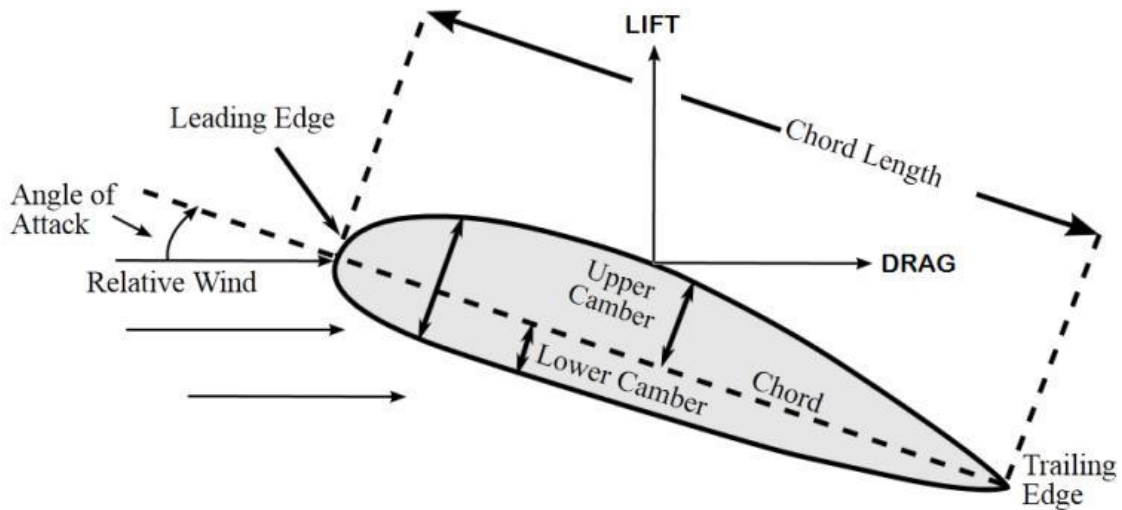


Figure 2.2.1: Airfoil

An airfoil, which is the wing's cross-sectional shape, is considered as a basic element in aerodynamics. The study of it clearly shows the fundamental concepts of aerodynamics. Moreover, simulation of various cases of wing's cross section gives exhaustive information for further development. The most common shape of the airfoil is presented in figure 2.2.1. As it can be seen from the figure, this shape is formed by the influence of its chamber line, chord line, leading and trailing edges, and so on. These terms will be described later.

Aerodynamic force is produced when an airfoil-shaped body travels through a fluid. The component of this force, parallel to the direction of motion, is termed the drag. The component perpendicular to the direction of motion is termed lift.

The lift of an airfoil is typically depended on its shape and angle of attack. The force on the airfoil, which is opposite direction to the deflection, is resulted as airfoil diverts the coming air in a suitable angle. This is the definition of the aerodynamic force and could be divided into two components, drag and lift. Despite that large portion of foil shapes demand a positive angle of attack to create lift, cambered airfoils could create lift at zero angle of attack. The higher pressure on one side and lower pressure on another side will occur due to curved streamlines, which is produced by "turning" of the air close to the airfoil. The difference in pressure and velocity, which can be explained by Bernoulli's principle, results in lower average velocity on the lower surface than on the upper surface for flow field about the airfoil.

Terms associated with the geometry of an airfoil:

- The 'leading edge' is the governing point of the airfoil. The leading edge coincides with stagnation point in zero angle of attack.
- The 'trailing edge' is the point at the end of the airfoil where the flow reunites.
- The 'chord line' is the direct line linking leading and trailing edges.

- The 'angle of attack' is the angle between the direction of the approaching flow and the chord line.
- The 'camber line' is the locus of point's midway between the upper and lower surfaces. It can be a straight line or not.
- The 'lift coefficient' is a dimensionless coefficient that relates to the density and velocity of fluid and to the lift force on the object to a reference area
- The 'drag coefficient' is a dimensionless coefficient that relates to the density and velocity of fluid and to the dragging force on the object to a reference area.
- The 'stall angle of attack' is the angle of attack at which the lift coefficient reaches its maximum and after which it starts to decrease.

2.3. Boundary Layers

Microscopically, the speed of air is zero at the boundary surface of a body immersed in moving fluid. In other words, fluid particles near the body's surface seem to 'stick' onto it [3]. Friction between fluid's moving particles and body's boundary generates the boundary layer, where the velocity of air is slowing down (close to zero) near to the

surface [3]. As we move away from the surface, fluid's (air's) speed increased to reach the corresponding flow speed. Moreover, it is crucial to define the boundary layer edge for the purposes of computation. However, boundary layer does not have definite edge. The effect of the boundary layer edge simply fades, which depends on viscosity, speed and surface roughness [3].

In figure 2.3.1, the main flow regimes are shown, this graph shows the how the viscosity of the fluid forms the thickness of the boundary layer which determines the 'stiffness' of the resistance to shear [13]. As the high of viscosity, the boundary layer is getting thicker. Study the phenomena of boundary layer mechanics analytically is very sophisticated and difficult, because of complication and chaotic.

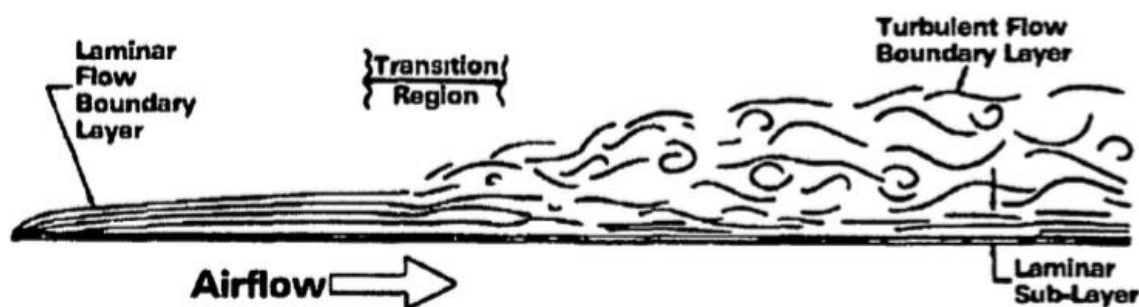


Figure 2.3.1: Development of the boundary layer

When the fluid gets first contact with the low speed, this phenomenon creates the layer of laminar boundary layer [3]. Initially,

the fluid runs over the body at exact and requested design, moving easily over one another systematically, getting quicker and quicker further far from the body until the point when it achieves free stream velocity [13]. This complex condition of many parameters forms the sophisticated reaction chain, which generates the chaotic movement. This condition leads to the formation of turbulent boundary layer. In order to define the type of flow, the common method of Reynolds number (Re) is used which is the ratio of the inertia and viscous forces. The formula is:

$$R_e = \frac{\rho VL}{\mu} \quad \text{eq. 2.4}$$

In this formula, V is the velocity (m/s), L is the length (m), ρ is the density (kg/m^3) and μ is the dynamic viscosity (kg/ms). There are approximate R_e value for laminar and turbulent flow, $R_e = 5 \times 10^5$ and more than $R_e = 2 \times 10^6$ respectively [13]. The difference in transition of the flow of laminar to turbulent does not by and large happen at a solitary very much characterized point, yet rather happens steadily so making the change area, between the two flow regimes.

In this way, there are two forms of boundary layers: first one is laminar flow, where the air goes easily in a streamlined way; second one

is turbulent flow. These two kinds of flow stream have distinctive characteristics. Essentially, the laminar layer creates less drag, yet the turbulent layer is less obligated to isolate from the bounding surface of the body [14]. Separational points are explained by setting apart process of fluid flow from body, which in case leads to the formation of a wake. A wake is considered as a field behind body, which is also submerged in a flow of fluid, this is indicated more plainly in Figure 2.3.2 [3].

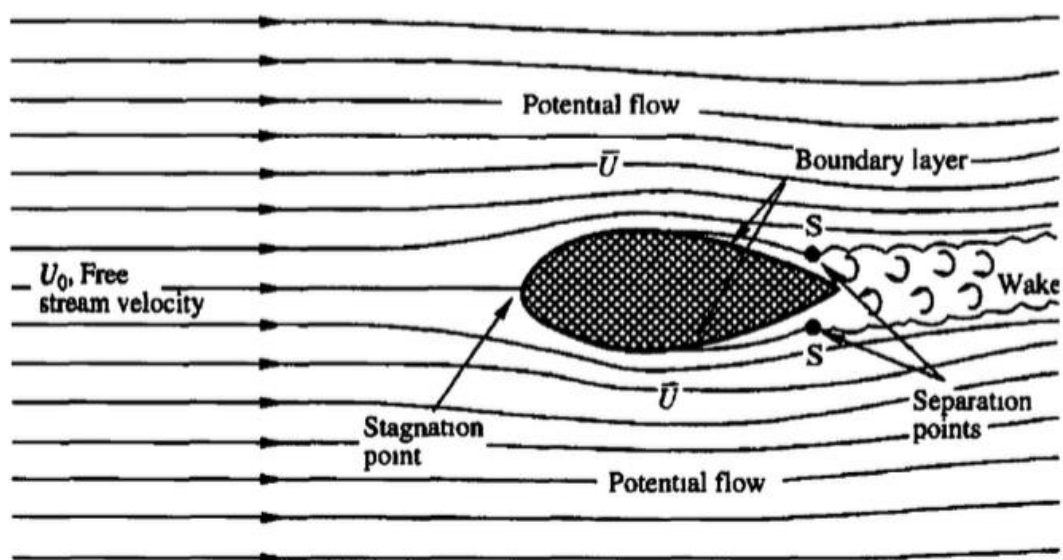


Figure 2.3.2: Development of a wake region

According to figure, wake region is started from separation points, where the boundary layer partition happens. Tail edges of the body shows a discontinuity of the surface. Consequently, the discontinuity and partition create a vortex area. This vortex area is called wake region.

2.4. Present Research Objectives

The objective of the present thesis is to combine a boundary layer model with a potential flow simulation. Specifically, the main steps of study are as follows:

1. Implement the one-way coupling of the potential flow with an appropriate boundary layer model
2. Implement two-way coupling with the same boundary layer model
3. Verify and benchmark the implementations against experimental results and similar computational tools like Pablo and Xfoil.

3. METHODOLOGY

For the implementation of one-way coupling, we are going to use a potential flow formulation solved using an IGA-BEM approach (Application of Isogeometric Analysis to Boundary Element Method) and the boundary layer model employed in Pablo [17]. Xfoil's boundary layer model will be employed for the two-way coupling.

3.1. The Inviscid Flow Model

Assuming inviscid formulation for the flow around an airfoil, the coupling between the boundary layer model and the inviscid formulation has to be described appropriately. The coupling contains two linked stages. Firstly, the boundary layer changes the body shape due to external flow and adds boundary layer thickness to the body's profile. Secondly, boundary layer model depends on the tangential velocity distribution, which is the solution of the inviscid problem. These two stages are considered when the inviscid and boundary layer flows are either one-way or two-way linked.

The inviscid flow problem can be solved using various methods. For instance, a 'finite difference discretization of the steady Euler equation on a grid around the airfoil' was used for the solution of inviscid flow [16]. Another method is a panel method, which is the

interest area of the project. The panel method is used in different programs such as Xfoil, Panda and Pablo. Moreover, the panel method differs regarding the singularity, which is utilized to present the velocity potential of the airfoil. They are, for example, sources, doublets and vortices. Detailed information about various panel methods and their differences can be found in [15].

The inviscid flow solution gives the tangential velocity distribution over airfoil's surface. Consequently, according to Bernoulli equation, pressure distribution can be evaluated. The lift coefficient can be computed by integrating the pressure over the surface of the body.

3.2. Pablo

Pablo is an instructive low-speed airfoil program written in MATLAB. It utilizes a one-way coupled inviscid and boundary layer model. The inviscid flow is solved using a panel method as in Xfoil or Panda [15]. However, the impact of the boundary layer on the inviscid flow is not considered. Pablo uses a linear vortex distribution for panel method. Moreover, Thwaites' one equation method and Head's equation method are used for laminar and turbulent flows respectively [10]. Michel's criterion is utilized regarding the transition criterion in Pablo [17].

3.2.1. Thwaites' Model

Thwaites' model is based on the integral momentum equation. Multiplying integral momentum equation by the Reynolds Number according to momentum thickness, it is obtained:

$$ReU_e \frac{d\theta^2}{dx} = 2[L - (2 + H)\lambda], \quad \text{eq. 3.1}$$

where $L = Re\theta U_e \frac{C_f}{2}$ and $\lambda = Re\theta^2 \frac{dU_e}{dx}$.

Then, Thwaites approximated the right-hand side linearly, which is:

$$2[1 - (2 + H)\lambda] \approx 0.45 - 6\lambda \quad \text{eq. 3.2}$$

When the equation 3.2 and the definition of λ are substituted into equation 3.1 and also performing some simplification, we obtain a differential equation:

$$Re \frac{d}{dx} (\theta^2 U_e^6) = 0.45 U_e^5 \quad \text{eq. 3.3}$$

where the value of θ is known:

$$\theta(x = 0) = \sqrt{\frac{0.075}{Re \frac{dU_e}{dx}(0)}}$$

By substituting and solving the integral according to 5th order Gauss quadrature [17], we obtain:

$$\int_{x_{i-1}}^{x_i} U_e^5 x(dx) \approx \frac{dx}{18} [5U_e^5 \left(x_m - \sqrt{\frac{3}{5} \frac{dx}{2}} \right) + 8U_e^5(x_m) + 5U_e^5 \left(x_m + \sqrt{\frac{3}{5} \frac{dx}{2}} \right)], \quad \text{eq. 3.4}$$

where $dx = x_i - x_{i-1}$ and $x_m = (x_i + x_{i-1})/2$.

Hence, θ is established, λ can be determined. Then H (shape factor) and C_f (skin friction coefficient) are calculated from semi-empirical formulas [17]:

$$H(\lambda) = 2.61 - 3.75\lambda + 5.24\lambda^2 \quad 0 < \lambda < 0.1$$

$$= 2.088 + \frac{0.0731}{\lambda + 0.14} \quad -0.1 < \lambda < 0$$

$$C_f = \frac{2L(\lambda)}{ReVe\theta}$$

$$L(\lambda) = 0.22 + 1.57\lambda - 1.8\lambda^2 \quad \text{for } 0 < \lambda < 0.1$$

$$= 0.22 + 1.402\lambda + \frac{0.018\lambda}{\lambda + 0.107} \quad \text{for } -0.1 < \lambda < 0$$

3.2.2. Head's Model

It is a common integral method, where analytic procedures have been performed before the numerical question is formulated. It is a sensibly precise and particularly quick technique. The Von Karman condition is employed by model and, as in the laminar case, some semi-experimental relations to close the framework. The technique has been determined as pursues.

The volume rate inside the boundary layer at point x is equal to:

$$Q(x) = \int_0^{\delta(x)} u dy \quad \text{eq. 3.5}$$

where $\delta(x)$ is the boundary layer thickness. Consolidating with the relocation thickness, it is obtained:

$$\delta^* = \delta - \frac{Q}{U_e}$$

The presented entrainment speed is:

$$E = \frac{dQ}{dx} = \frac{d}{dx} U_e (\delta - \delta^*) \quad \text{eq. 3.6}$$

Which is:

$$E = \frac{d}{dx} (U_e \theta H_l)$$

With:

$$H_l = \frac{\delta - \delta^*}{\theta}$$

Head accepted that the dimensionless entrainment speed E/U_e depends just on H_l and that H_l , thus, is a function of H .

$$\frac{1}{U_e} \frac{d}{dx} (U_e \theta H_l) = 0.0306 (H_l - 3)^{-0.6169} \quad \text{eq. 3.7}$$

$$H_l = k(H) = 3.3 + 0.8234(H - 1.1)^{-1.287} \text{ for } H \leq 1.6$$

$$= 3.3 + 1.5501(H - 0.6778)^{-3.064} \text{ for } H > 1.6$$

The equation used to explain for the questions θ , H_l , H , and C_f is the Ludwig-Tillman skin friction law:

$$C_f = 0.246 * (10^{-0.678H}) Re_\theta^{-0.268} \quad \text{eq. 3.8}$$

3.2.3. Michel's Criterion

The criterion states that conversion process begins at an explicit Reynolds number dependent on the distance x from the boundary layer. The transition Reynolds number relies upon numerous aspects, the most imperative being the gradient of pressure forced on the limit layer by the inviscid stream and the surface harshness.

In cases when the heat transfer is not seen in incompressible flows, Michel [17] analyzed an assortment of information and reasoned that, for airfoil-type applications, the conversion is anticipated when:

$$Re_{\theta} > Re_{\theta_{max}} = 1.174 \left(1 + \frac{22.4}{Re_x} \right) (Re_x)^{0.46}, \quad \text{eq. 3.9}$$

where $Re_{\theta} = ReU_e\theta$ and $Re_x = ReU_ex$.

This relation accounts for the impact of the pressure gradient, in light of the fact that the energy thickness develops more quickly in a positive pressure gradient. Nevertheless, it excludes the impact of surface roughness, yet being founded on information gone up against airfoils; it ought to be great for wing investigation. Usage of introduced criterion uncovers the situations where the outside stream speed is not monotone past the suction crest, the capacity is not monotone either, and can in this way, have a few zeros. Since progress is anticipated

when the capacity vanishes, this can result in a brokenness in the arrangement regarding the plan parameters, as showed on the accompanying precedent.

3.3. IGA-BEM Solver

In this subsection, the IGA-BEM solver is adopted, which is presented in [5], to employ it for the potential flow analysis. The IGA-BEM solver is introduced to this thesis project because of its satisfactory results against analogous results of low-order panel method described in [10]. Large number of elements were employed in low-order panel method while the IGA-BEM method utilized less degrees of freedom for the same result. The comparison of potential distribution around NACA-4412 profile in IGA-BEM solver with low-order panel method is presented graphically in [5].

3.3.1. Governing Equations

In this case, there is a 2D body with boundary marked as $\partial\Omega_B$ in Figure 3.3.1.1. The body is moving in an ideal fluid of infinite scope with constant speed of \vec{U}_B . This problem in a body-fixed coordinate system O_{xy} is equivalent to a uniform stream with velocity $\nabla\Phi_\infty = \vec{U}_\infty = -\vec{U}_B$, and where the far-field asymptotic form of the velocity potential of the

flow $\Phi(P)$, at point $P = (x, y)$ is $\Phi_\infty(P) = u_\infty x + v_\infty y$. Thus, the solution of the boundary-value problem (BVP) is potential $\Phi(P)$:

$$\nabla^2 \Phi = 0, P = (x, y) \in \Omega, \quad \text{eq. 3.10}$$

$$\frac{\partial \Phi}{\partial n} = 0, P \in \partial \Omega_B,$$

$$\Phi - (u_\infty x + v_\infty y) \rightarrow 0, \text{ as } x^2 + y^2 \rightarrow \infty$$

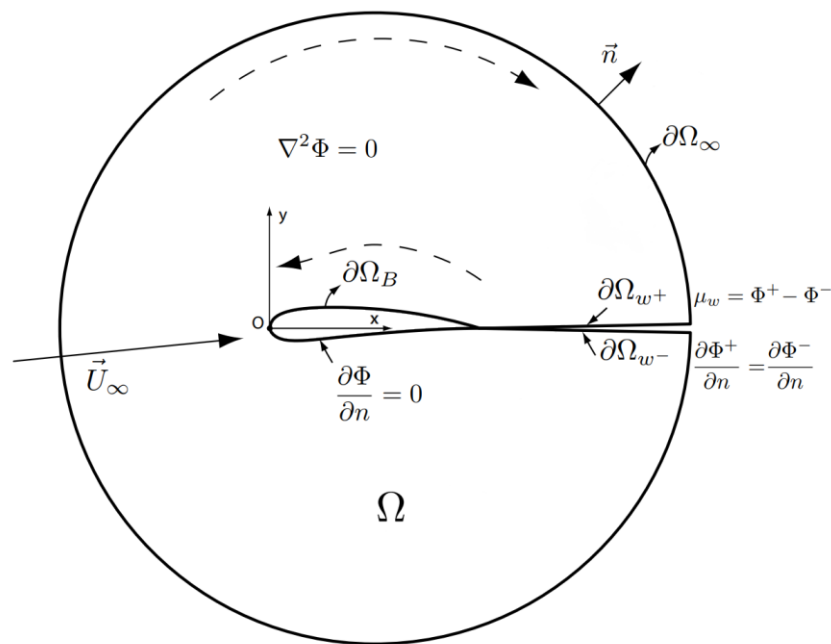


Figure 3.3.1.1: A hydrofoil in a flow

In this equation Ω is the fluid domain outside the boundary and \vec{n} is representing the unit normal vector on $\partial \Omega_B$. In order for the flow going around the hydrofoil to obtain a physical meaning, the circulation has to be non-zero and appropriately adjusted until the flow leaves the trailing edge smoothly, thus, the defining the difference between potential flows around a smooth body and a hydrofoil. To be specific,

Prandtl, on the basis of Kelvin's theorem, concluded that if an airfoil in an ideal fluid, which started its motion from rest, is later found to have non-zero circulation Γ , then the component of the borders of the fluid coinciding with the airfoil initially, has to, at a later time, coincide at with the union of the airfoil surface and a surface, also so-called wake, embedded in the fluid with circulation of $-\Gamma$. In the 2D case, without the loss of generality, the location and shape of the wake can be taken to be a straight line extending to infinity and emanating from the trailing edge. That makes the line a force-free boundary, which the normal fluid velocity and the pressure should exhibit no jump along at. To be more accurate, we can write the following:

$$\frac{\partial\Phi^+}{\partial n} = \frac{\partial\Phi^-}{\partial n}, P \in \partial\Omega_\omega: \textit{kinematic boundary condition}$$

$$p^+ = p^-, P \in \partial\Omega_\omega: \textit{dynamic boundary condition}$$

Therefore, in equation 3.11, by applying Green's second identity between potential $\Phi(P), P \in \Omega$, and the fundamental solution, $G(P, Q) = \left(\frac{1}{2\pi}\right) \ln\|P - Q\|$, of the 2D Laplace equation (3.10) the reformulated formula for BVP is obtained, considering the wake-sheet conditions.

$$\frac{\phi(P)}{2} + \int_{\partial\Omega_B} \phi(Q) \frac{\partial G(P,Q)}{\partial n_Q} ds_Q - \mu_\omega \int_{\partial\Omega_\omega} \frac{\partial G(P,Q)}{\partial n_Q} ds_Q = \phi_\infty(P), P \in \partial\Omega_B \setminus P_{TE} \textit{ eq. 3.11}$$

$$\phi(P) = \Phi(P) - \Phi_\infty(P)$$

$$\begin{aligned} & \frac{\phi(P)}{2} + \int_{\partial\Omega_B} \phi(Q) \frac{\partial G(P,Q)}{\partial n_Q} ds_Q - \mu_\omega \int_{\partial\Omega_\omega} \frac{\partial G(P,Q)}{\partial n_Q} ds_Q = \\ & - \int_{\partial\Omega_B} (\vec{U}_\infty \cdot \vec{n}(Q)) G(P,Q) ds_Q, \quad P \in \partial\Omega_B \setminus P_{TE} \quad \underline{eq. 3.12} \end{aligned}$$

After solving equation (3.11) or (3.12), it is now possible to calculate, using Bernoulli's equation, the hydrofoil's pressure coefficient c_p :

$$c_p := \frac{p - p_\infty}{\frac{1}{2} \rho |\vec{U}_\infty|^2} = 1 - \frac{v_t^2}{|\vec{U}_\infty|^2}$$

The main aim of this methodology is to solve the boundary integral equations (3.11) and (3.12) numerically. The philosophy of IGA is equal to approximating the amounts of field coming from the BVP in question via the same basis geometry description of the body-boundary involved. In this specific case, the dependent variables are the total potential $\Phi(P), P \in \partial\Omega_B$ (equation 3.11) or the perturbation potential $\varphi(P), P \in \partial\Omega_B$ (equation 3.12). For this purpose, it is presumed that the body boundary $\partial\Omega_B$ is able to be displayed as a closed parametric NURBS curve $r(t), t \in [0,1]$, the derivative vector is defined satisfactory and does not vanish, with the exception of the trailing edge: $r(0) = r(1)$, where the derivative vector is not characterized.

For the purpose of simplicity notations and applying the kernel function, the equation 3.12 is rewrote:

$$\frac{\phi(t)}{2} + \int_l \phi(t) K(t, \tau) d\tau - \frac{\mu_\omega}{2\pi} \arctan\left(\frac{y(t)-y_e}{x(t)-x_e}\right) = g(t), \quad t \in (0,1) \quad \text{eq. 3.13}$$

Consisting in projecting spline space through interpolation at a set of collocation points, which are chosen to be the Greville abscissas associated with the knot vector a collocation scheme is adopted. Consequently, a new modified linear system with unknown coefficients $\phi_i, i = 0, \dots, n + l$ is obtained:

$$\frac{1}{2} \sum_{i=0}^{n+l} \phi_i M_{i,k}^{(l)}(t_j) + \sum_{i=0}^{n+l} \phi_i q_i(t_j) - \frac{(\phi_{n+l} - \phi_0)}{2\pi} \arctan\left(\frac{y(t)-y_e}{x(t)-x_e}\right) = g(t_j), \quad j = 0, \dots, n + l$$

eq. 3.14

Thus, solving the equation (3.14) gives the values of $\phi_i, i = 0, \dots, n + l$, and those values are able to be used in calculating easily the tangential velocity on the hydrofoil by using the derivatives of the rational B-spline functions $M_{i,k}^{(l)}(t)$, making it not necessary to resort to the finite difference system:

$$v_t = \vec{U}_\infty \cdot \vec{t} + \frac{\partial \phi}{\partial s} = \vec{U}_\infty \cdot \vec{t} + \frac{1}{\|\dot{r}(t)\|} \sum_{i=0}^{n+l} \phi_i \frac{dM_{i,k}^{(l)}(t)}{dt},$$

where \vec{t} denotes the unit-tangent vector of $r(t)$.

3.4. Xfoil

The Xfoil program's framework comprises of a gathering of menu-driven functions, which are shown in figure 3.4.1, that allow executing inviscid and viscous calculations. Sustaining commands of panels' distribution, geometry control, and graphical interface are likewise guided using the same menu. The "Geometry Manipulator" permits unequivocal control of camber, thickness, leading edge, trailing edge and so forth. This is exceptionally helpful when geometric limitations have to be built and can be extremely compelling for accomplishing certain streamlined functions too.

```

SAVE f Write airfoil to labeled coordinate file
PSAV f Write airfoil to plain coordinate file
ISAV f Write airfoil to ISES coordinate file
MSAV f Write airfoil to MSES coordinate file
REVE Reverse written-airfoil node ordering

LOAD f Read buffer airfoil from coordinate file
NACA i Set NACA 4,5-digit airfoil and buffer airfoil
INTE Set buffer airfoil by interpolating two airfoils
NORM Buffer airfoil normalization toggle
XYCM rr Change CM reference location, currently 0.25000 0.00000

BEND Display structural properties of current airfoil

PCOP Set current-airfoil panel nodes directly from buffer airfoil points
PANE Set current-airfoil panel nodes ( 160 ) based on curvature
.PPAR Show/change paneling

.PLOP Plotting options

WDEF f Write current-settings file
RDEF f Reread current-settings file
NAME s Specify new airfoil name
NINC Increment name version number

Z Zoom | (available in all menus)
U Unzoom |

XFOIL c>

```

Figure 3.4.1. Xfoil interface

Xfoil utilizes the viscous formulation for laminar and turbulent flows, which is based on the integral momentum and kinetic energy differential equations [17].

```

XFOIL c> naca 4412
Max thickness = 0.120035 at x = 0.300
Max camber = 0.040000 at x = 0.402

Buffer airfoil set using 331 points
Blunt trailing edge. Gap = 0.00252

Paneling parameters used...
Number of panel nodes 160
Panel bunching parameter 1.000
TE/LE panel density ratio 0.150
Refined-area/LE panel density ratio 0.200
Top side refined area x/c limits 1.000 1.000
Bottom side refined area x/c limits 1.000 1.000

XFOIL c> pane

Blunt trailing edge. Gap = 0.00252

Paneling parameters used...
Number of panel nodes 160
Panel bunching parameter 1.000
TE/LE panel density ratio 0.150
Refined-area/LE panel density ratio 0.200
Top side refined area x/c limits 1.000 1.000
Bottom side refined area x/c limits 1.000 1.000

XFOIL c> oper

.OPERi c> v

Enter Reynolds number r> 1000000

M = 0.0000
Re = 1000000

.OPERv c> pacc

Polar 1 newly created for accumulation
Airfoil archived with polar: NACA 4412

Enter polar save filename OR <return> for no file s> original_xfoil_result.txt
New polar save file available

Enter polar dump filename OR <return> for no file s> ref_orig.txt
New polar dump file available

Polar accumulation enabled

.OPERva c> alfa 1

```

```

XFOIL c> load xfoil.txt

Plain airfoil file

Enter airfoil name s> NACA 4412 tang vel input data

Number of input coordinate points: 400
Clockwise ordering
Max thickness = 0.120200 at x = 0.298
Max camber = 0.038167 at x = 0.421

LE x,y = -0.00023 0.00313 | Chord = 1.00024
TE x,y = 1.00000 0.00000 |

Current airfoil nodes set from buffer airfoil nodes ( 400 )

XFOIL c> oper

.OPERi c> v

Enter Reynolds number r> 1000000

M = 0.0000
Re = 1000000

.OPERv c> iter
Current iteration limit: 10

Enter new iteration limit i> 20

.OPERv c> pacc

Polar 1 newly created for accumulation
Airfoil archived with polar: NACA 4412 tang vel input data

Enter polar save filename OR <return> for no file s> adapted_xfoil_result.txt
New polar save file available

Enter polar dump filename OR <return> for no file s> ref_adap.txt
New polar dump file available

Polar accumulation enabled

.OPERva c> alfa 1

```

(a)

(b)

Figure 3.4.2: Set up procedure for the (a) original xfoil;
(b) adapted xfoil viscous formulation

In this subsection, Xfoil's source code was modified to compare the performance capability of original and adapted Xfoil. The modification is based on a tangential velocity distribution data. For the case of Xfoil tool, the tangential velocities were calculated within the program itself, while for the adapted method, the data was taken from the IGA-BEM solver method, which was calculated using MATLAB and used as an input for the source code.

Initially, the original Xfoil program was used to perform the viscous formulation of potential flow. With the integrated NACA 4 digits library, just by calling the airfoil name in the command line, in our

case, *NACA 4412*, the shape of the airfoil is formulated automatically. Then, *pane* command is used to achieve a better panel node distribution by smoothing the sharp edges of high curvature areas. Afterward, *OPER* command is utilized to activate viscous mode, which asks to enter the value of Reynolds number and angle of attack. Moreover, *PACC* command is employed to extract data in the txt format. Thus, Xfoil produces the graphics of the potential flow about the airfoil with the boundary layer. For the adapted Xfoil program, almost all command and functions used are the same except for the input of airfoil shape. Instead, the *LOAD* command is employed to add the point coordinates of *NACA 4412* in txt format. The graphical part of source code was excluded from the source code, as the extraction of viscous calculation results in txt format is applicable. The whole set up procedures for both models are represented in figure 3.4.2. The modified source code written in FORTRAN language is given below:

SUBROUTINE QVFUE

```

C-----
C  Sets panel viscous tangential velocity
from viscous Ue
C-----
  INCLUDE 'XFOIL.INC'
C
  DO 1 IS=1, 2
    DO 10 IBL=2, NBL(IS)
      I = IPAN(IBL, IS)
      QVIS(I) = VTI(IBL, IS)*UEDG(IBL,
IS)
  10 CONTINUE
  1 CONTINUE
C
  RETURN
  END

```

SUBROUTINE QISET

```

C-----
C  Sets inviscid panel tangential velocity
for current alpha.
C-----
  INCLUDE 'XFOIL.INC'
C
  COSA = COS(ALFA)
  SINA = SIN(ALFA)
C
  OPEN (99, file="tangVelocity.txt")
  PRINT *, N
  DO 5 I=1, N-1
    READ (99, *) QINV(I)
    PRINT *, QINV(I)
C$$$$$$   QINV (I) =
COSA*QINVU(I,1) + SINA*QINVU(I,2)
QINV_A(I) = -SINA*QINVU(I,1) +
COSA*QINVU(I,2)
  5 CONTINUE
    QINV(N)=QINV(N-1)
  CLOSE (99)
C
  RETURN
  END

```

4. RESULTS AND DISCUSSION

4.1. Results of Inviscid Flow Model in Pablo and IGA

In this chapter, the results of one-way coupling consist of four parts regarding the angles of attack used to calculate lift and drag coefficients for a different number of panels and degree of freedom in Pablo and IGA respectively. The angles of attack utilized to perform calculations are 1° , 3° , 5° and 7° . Furthermore, this section contains the figures of lift and drag coefficients against the number of panels and degree of freedom. As a benchmark, the following input data was considered: $Re = 1 \times 10^6$, Chord length = 1 m, Velocity = 1 m/s.

Table 4.1.1. Results of C_l and C_d for 1° angle of attack (Pablo and IGA)

						100points	200points	400points
angle of attack	number of panels	CL pablo (vortex)	CD pablo	DOF	CL (IGA)	CD (IGA)	CD (IGA)	CD (IGA)
1	80	0,61271	0,0075	83	0,64881	0,0082	0,008	0,0081
1	200	0,6322	0,0081	163	0,64436	0,0083	0,0081	0,0082
1	400	0,6339	0,0082	243	0,64277	0,0084	0,0081	0,0082
1	998	0,6348	0,0083	323	0,64197	0,0084	0,0081	0,0082

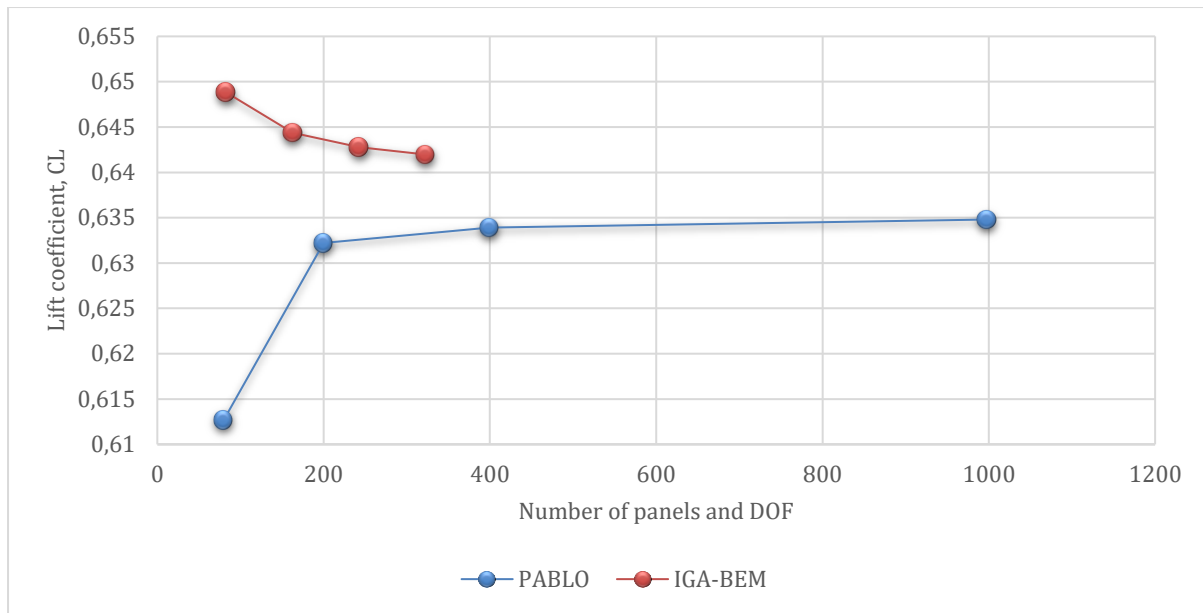


Figure 4.1.1: C_l against number of panels and DOF of an NACA 4412 airfoil for 1° angle of attack (Pablo and IGA-BEM)

In table 4.1.1, the results of lift and drag coefficients for Pablo and IGA methods are presented. The considered angle of attack is 1° . It is seen that the value of lift coefficient converges as the number of panels increases from 80 to 998 in the case of Pablo, while the IGA solver's result is satisfactory even with the low degree of freedom ($n=83$). Graphically, according to figure 4.1.1, the variation of lift coefficients against the number of elements used in both models considerably differs even with the same range of limits regarding C_l .

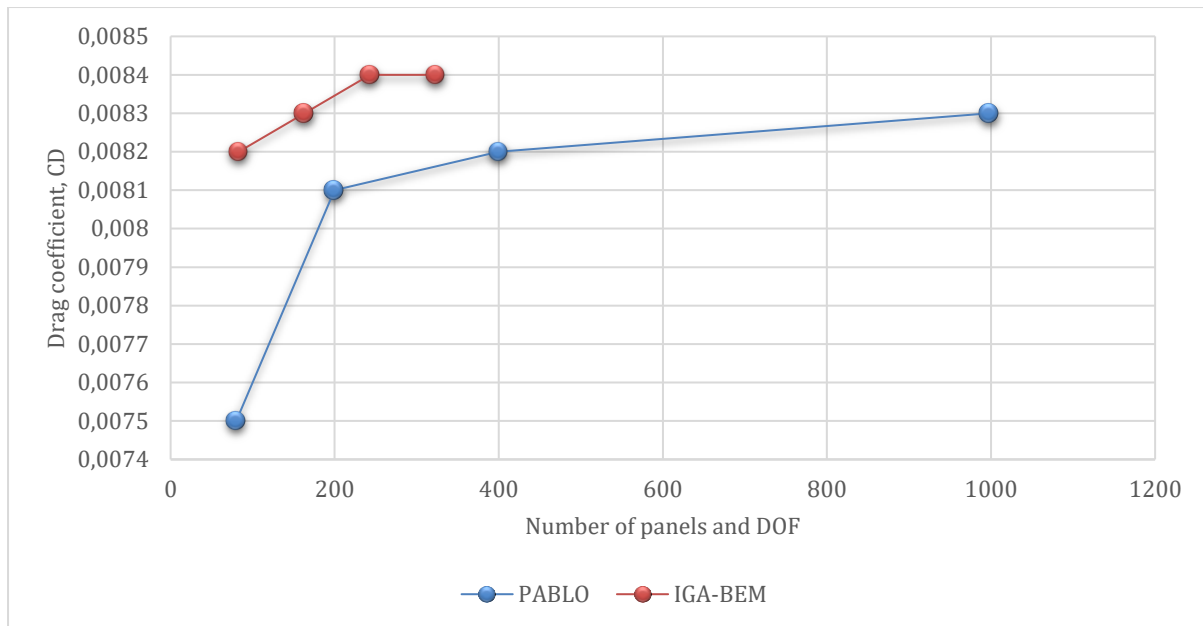


Figure 4.1.2: C_d against number of panels and DOF of an NACA 4412 airfoil for 1° angle of attack (PABLO and IGA-BEM)

The same feature can be found for the drag coefficient analysis. However, for the computation of drag coefficient in IGA solver, additional control points ($P = 100, 200, 400$) were introduced to observe its effect. It is obvious that the addition of more control points to the solver leads to the more accurate outcome. However, even with $P = 100$ and $n = 83$, the IGA solver's drag coefficient shows an adequate result. The variation range of drag coefficients for two methods can be found in figure 4.1.2.

In this way, the results provided by Pablo and IGA are compared for the rest test cases. Each test case for the rest angles of attack describes the sensitivity of the results with respect to the number of elements

(number of panels and degree of freedom) and to the lift and drag coefficients. All corresponding figures and tables are shown below:

Table 4.1.2. Results for C_l and C_d for 3° angle of attack (Pablo and IGA)

angle of attack	number of panels	CL pablo (vortex)	CD pablo	DOF	CL (IGA)	CD (IGA)	CD (IGA)	CD (IGA)
3	80	0,8649	0,0076	83	0,89374	0,0078	0,0078	0,0078
3	200	0,8718	0,0077	163	0,88728	0,0078	0,0077	0,0077
3	400	0,874	0,0077	243	0,88498	0,0078	0,0077	0,0077
3	998	0,8753	0,0077	323	0,88383	0,0078	0,0077	0,0077

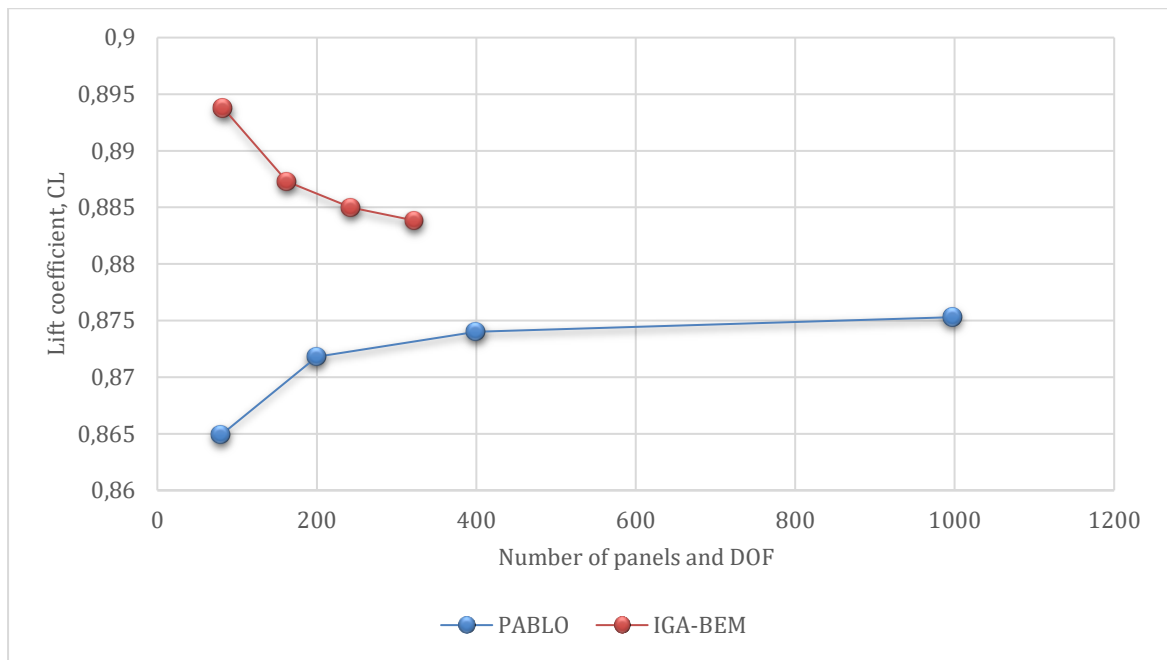


Figure 4.1.3: C_l against number of panels and DOF of an NACA 4412 airfoil for 3° angle of attack (Pablo and IGA-BEM)

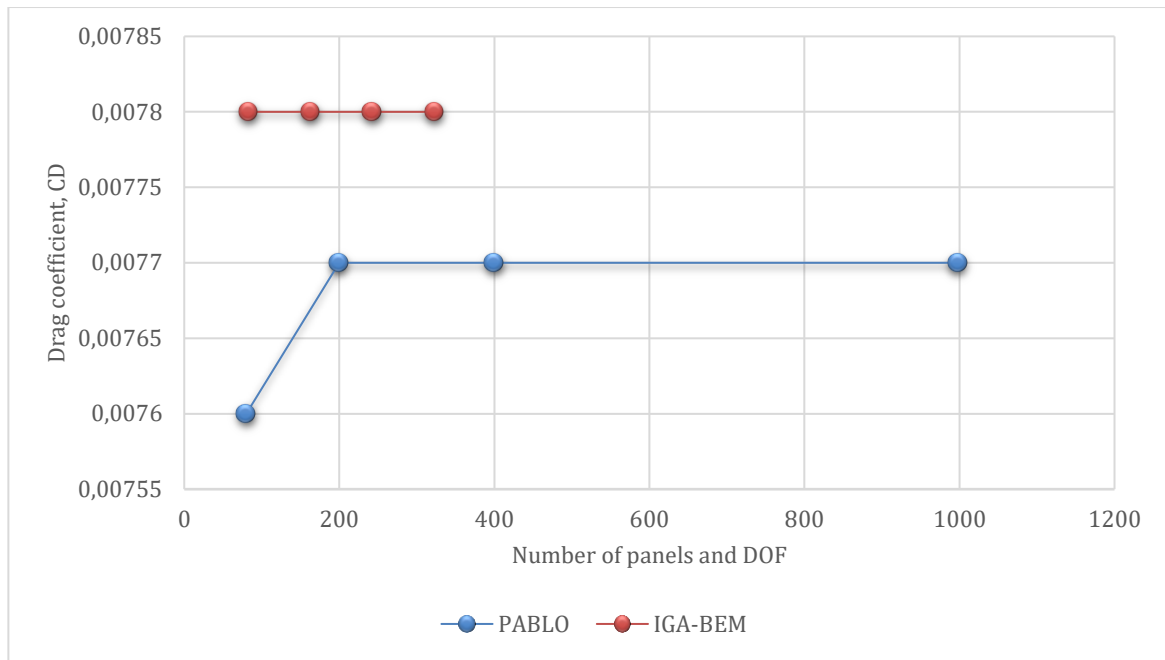


Figure 4.1.4: C_d against number of panels and DOF of an NACA 4412 airfoil for 3° angle of attack (Pablo and IGA-BEM)

Table 4.1.3. Results for C_l and C_d for 5° angle of attack (Pablo and IGA)

						100points	200points	400points
angle of attack	number of panels	CL pablo (vortex)	CD pablo	DOF	CL (IGA)	CD (IGA)	CD (IGA)	CD (IGA)
5	80	1,1017	0,0092	83	1,1415	0,0093	0,0095	0,0096
5	200	1,1103	0,0095	163	1,1311	0,0093	0,0095	0,0096
5	400	1,1131	0,0095	243	1,1274	0,0093	0,0095	0,0096
5	998	1,1147	0,0095	323	1,1256	0,0093	0,0095	0,0096

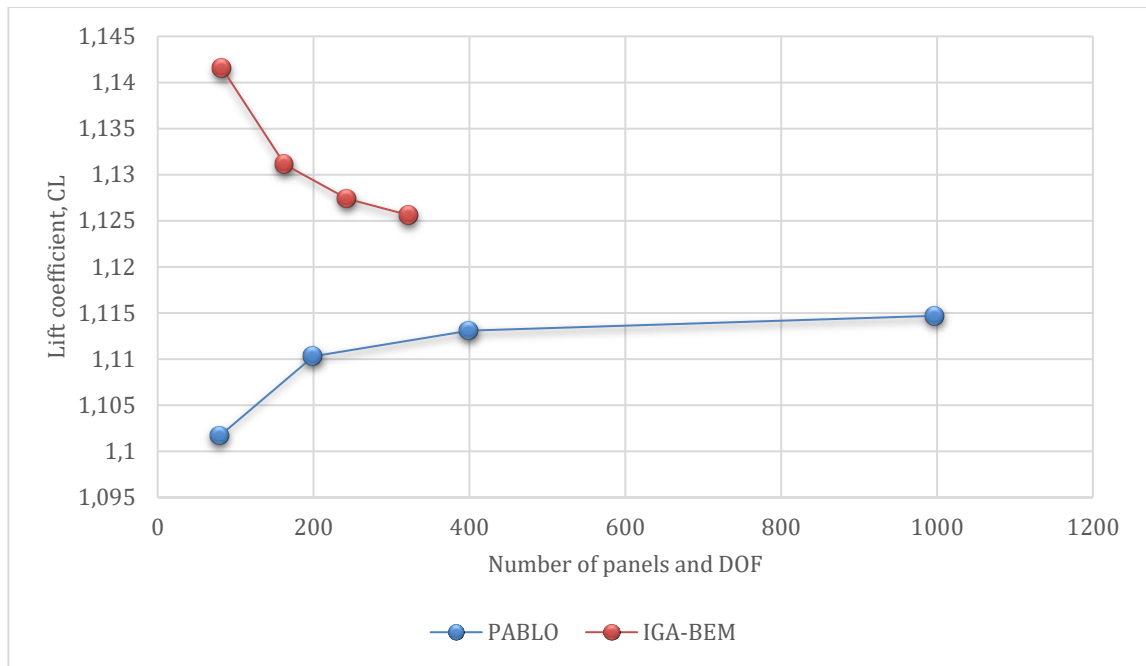


Figure 4.1.5: C_L against number of panels and DOF of an NACA 4412 airfoil for 5° angle of attack (Pablo and IGA-BEM)

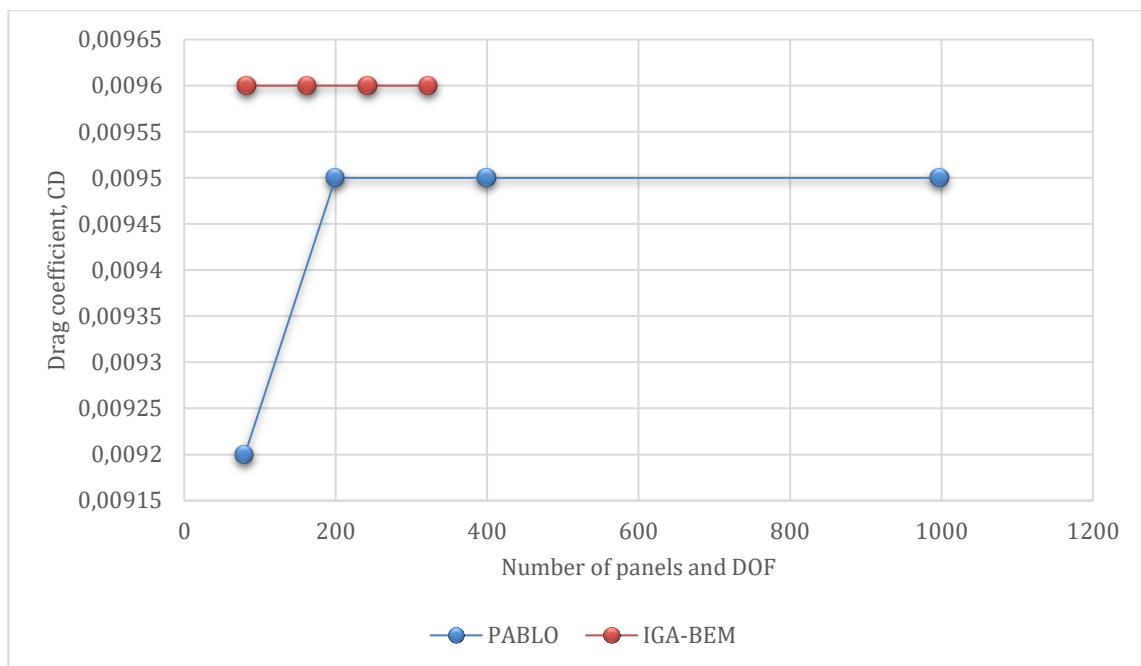


Figure 4.1.6: C_D against number of panels and DOF of an NACA 4412 airfoil for 5° angle of attack (Pablo and IGA-BEM)

Table 4.1.4. Results for C_l and C_d for 7° angle of attack (Pablo and IGA)

						100points	200points	400points
angle of attack	number of panels	CL pablo (vortex)	CD pablo	DOF	CL (IGA)	CD (IGA)	CD (IGA)	CD (IGA)
7	80	1,337	0,012	83	1,3917	0,0152	0,0126	0,0128
7	200	1,3474	0,0124	163	1,3754	0,0151	0,0126	0,0128
7	400	1,3508	0,0123	243	1,3698	0,0151	0,0126	0,0128
7	998	1,3528	0,0127	323	1,3669	0,0151	0,0126	0,0128

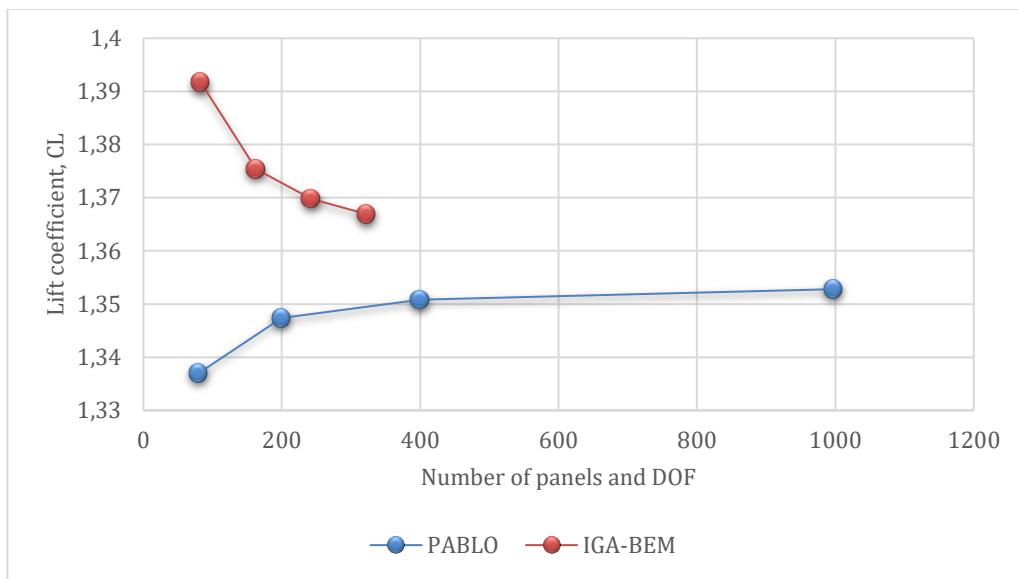


Figure 4.1.7: C_l against number of panels and DOF of an NACA 4412 airfoil for 7° angle of attack (Pablo and IGA-BEM)

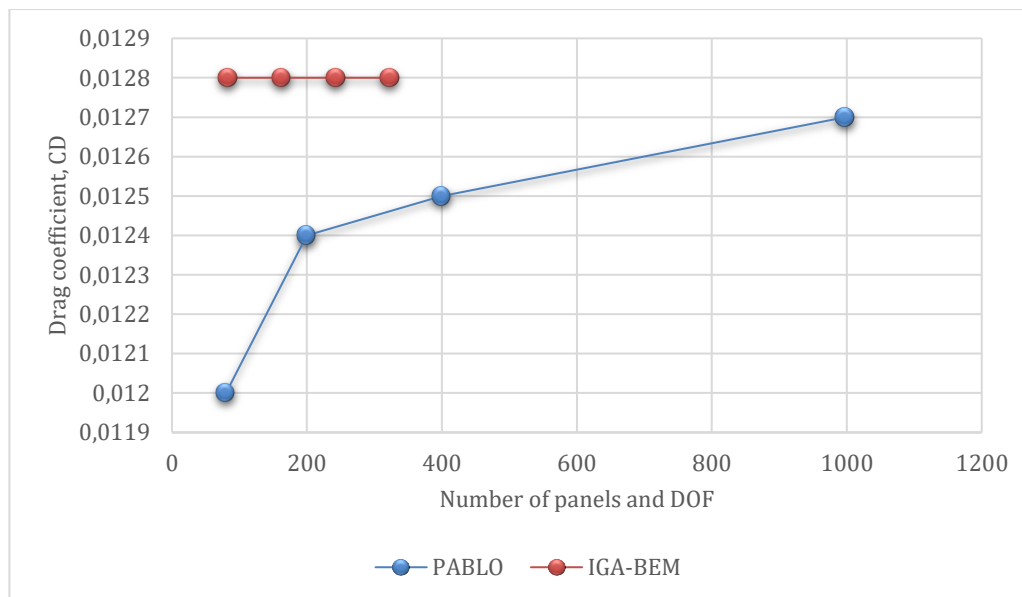


Figure 4.1.8: C_d against number of panels and DOF of an NACA 4412 airfoil for 7° angle of attack (Pablo and IGA-BEM)

4.2. Results of Viscous Flow Model in Xfoil

The graphics of original Xfoil for viscous flow analysis are depicted in figure 4.2.1. In figures 4.2.2 and 4.2.3, the plot of lift coefficient and drag coefficient against number of points for original and adapted Xfoil is represented respectively. The iteration number of original Xfoil's result was 8 iterations, while for the convergence of the adapted Xfoil's solution, 13 iterations were required. The iteration results can be seen from figures 1 and 2, in appendices. The result of adapted Xfoil is considered to be more stable and accurate than original Xfoil's result. Because, the tangential velocity distribution data coming from IGA-BEM solver is accurate.

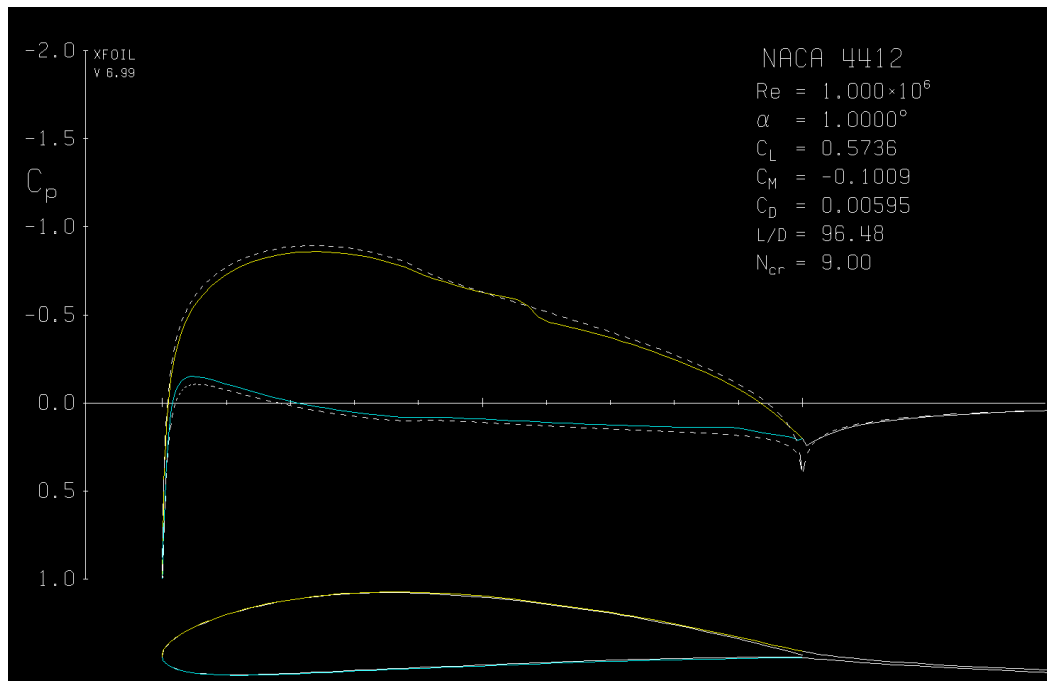


Figure 4.2.1. Original Xfoil plot

Table 4.2.1: Results of C_l for 1° angle of attack

Number of points	CL (original)	CL (adapted)
81	0,5822	0,5804
120	0,581	0,5805
160	0,5801	0,5802
200	0,5824	0,5802
400	0,5376	0,5368

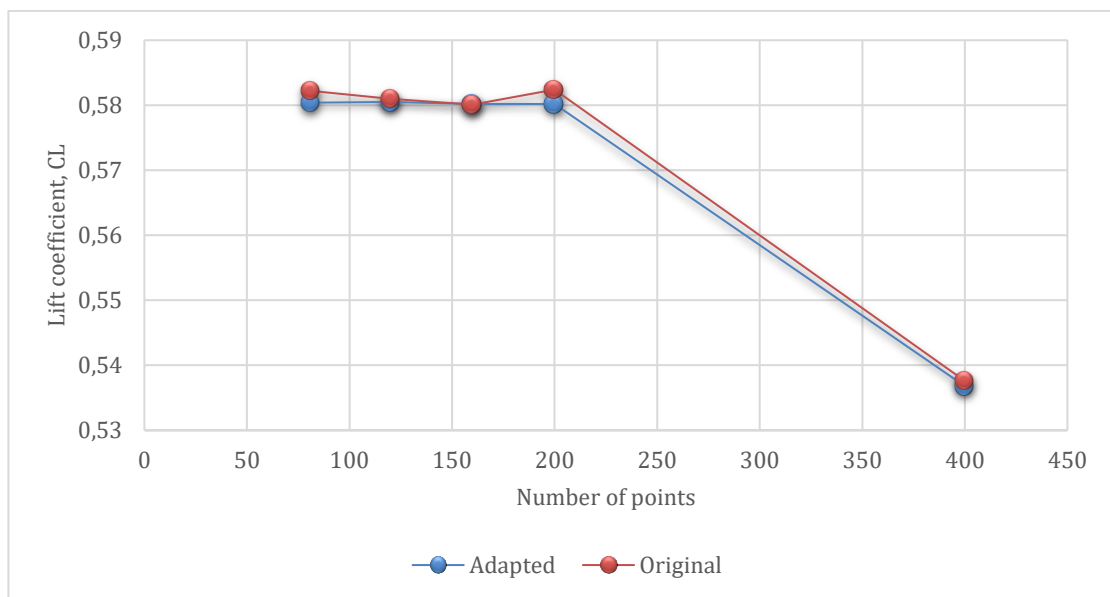


Figure 4.2.2. C_l against number of points of an NACA 4412 airfoil for 1° angle of attack

Table 4.2.2: Results of C_d for 1° angle of attack

Number of points	CD (original)	CD (adapted)
81	0,00584	0,00587
120	0,00585	0,00588
160	0,00586	0,00589
200	0,00595	0,00589
400	0,00585	0,00583

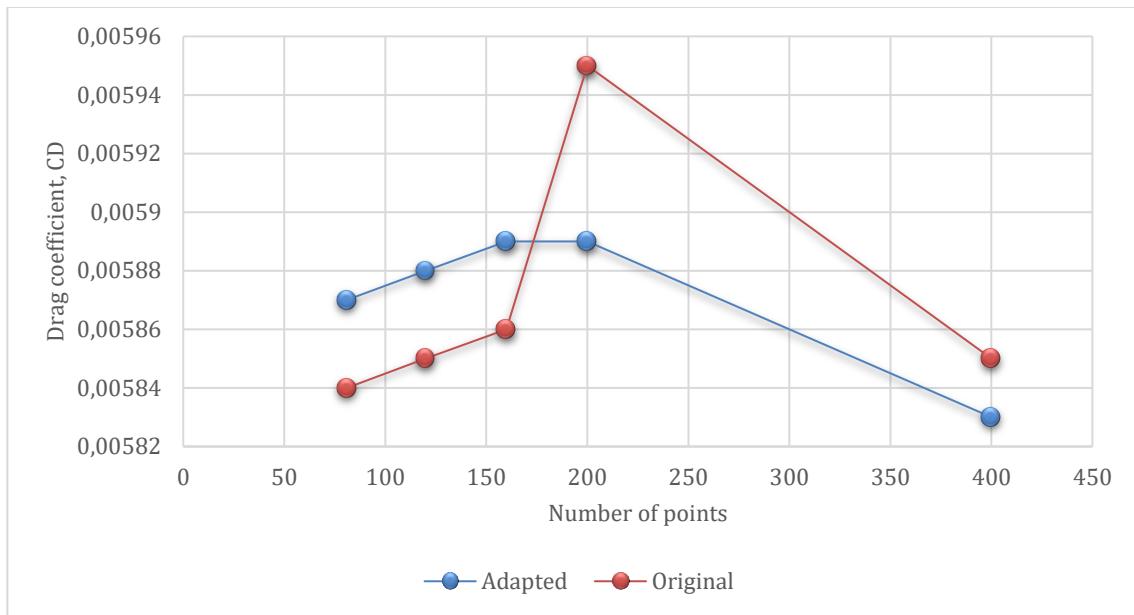


Figure 4.2.3. C_d against number of points of an NACA 4412 airfoil for 1° angle of attack

In general, as the boundary layer model modifies the shape of the airfoil in the viscous formulation of potential flow, the results of two-way coupling differs and considered to be more accurate in comparison with one-way coupling methods modelled by Pablo and IGA solver. Also, the turbulent flow models differ, for instance, Xfoil program can handle a thin separated flow region, although Head's equation in Pablo cannot. Moreover, the drag coefficient computation in Xfoil comprises the integration of the pressure distribution and boundary layer friction, instead in Pablo, the Squire-Young formula is employed for the calculation of drag coefficient.

5. CONCLUSION

In the present work, the problem of potential flows about airfoils/hydrofoils has been solved with one-way and two-way boundary layer models. One-way coupled boundary layer model was modeled by using Pablo and IGA-BEM solver. This procedure has been successfully applied for the computation of lift and drag coefficients with respect to the number of elements used. The results of both models have been compared. On the whole, IGA-BEM model has represented more satisfactory results in terms of the used number of elements. Two-way coupled boundary layer model has been constructed utilizing the Xfoil program. Furthermore, the adapted Xfoil executable program has been developed through the usage of tangential velocities taken from IGA-BEM solver as the input to the source code of the original Xfoil program. The two-way coupling solution algorithm with adapted Xfoil program could predict the aerodynamic coefficients more accurately.

Overall, IGA-BEM model is considered to be effective because it utilized less number of used DOF rather than traditional tool as Pablo. For the Xfoil analysis, adapted Xfoil's results are expected to be accurate than original results due to accurate inviscid flow solution coming from IGA-BEM solver.

REFERENCES

- [1]. Benra, F. K., Dohmen, H. J., Pei, J., Schuster, S., and Wan, B. (2011). *A comparison of one-way and two-way coupling methods for numerical analysis of fluid-structure interactions*. Journal of applied mathematics.
- [2]. O'Reilly, Eugene. (2006). *Analysis of boundary layers through computational fluid dynamics and experimental analysis*. Diss. Dublin City University.
- [3]. Douglas, J. F., Gasiorek, J. M. and Swaffield, J. A. (1998). *Fluid Mechanics*, 3rd Edition. Longman Singapore Publishers Ltd , Singapore.
- [4]. Hughes, T. J., Cottrell, J. A., and Bazilevs, Y. (2005). Isogeometric analysis: CAD, finite elements, NURBS, exact geometry and mesh refinement. *Computer methods in applied mechanics and engineering*, 194, (39-41), 4135-4195.
- [5]. Kostas, K. V., Ginnis, A. I., Politis, C. G., and Kaklis, P. D. (2017). Shape-optimization of 2D hydrofoils using an Isogeometric BEM solver. *Computer-Aided Design*, 82, 79-87.
- [6]. Schafer, M., Sieber, G., Sieber, R., and Teschauer, I. (2001). *Coupled Fluid-Solid Problems: Examples and Reliable Numerical Simulation*, WA Wall, K. Trends in Computational Structural Mechanics, CIMNE, Barcelona.
- [7]. Nobile, F. (2001). *Numerical approximation of fluid-structure interaction problems with application to haemodynamics*. Ph.D. thesis, EPFL, Switzerland.
- [8]. Peric, D., and Dettmer, W. G. (2005). *A computational strategy for interaction of fluid flow with spatial structures*. In Proceedings of the 5th International Conference on Computational of Shell and Spatial Structures (IASS IACM '05).
- [9]. Piperno, S., Farhat, C., and Larrouturou, B. (1995). *Partitioned procedures for the transient solution of coupled aeroelastic problems Part I: Model problem, theory and two-dimensional application*. *Computer methods in applied mechanics and engineering*, 124(1-2), 79-112.
- [10]. Moran, J. (2003). *An introduction to theoretical and computational aerodynamics*. Courier Corporation.
- [11]. Thwaites, B., and Street, R. E. (1960). *Incompressible aerodynamics*. *Physics Today*, 13, 60.
- [12]. Anderson, J. (2010). *Fundamentals of Aerodynamics* (McGraw-Hill Series in

Aeronautical and Aerospace Engineering).

- [13]. Le Good, G. M., and Garry, K. P. (2004). *On the use of reference models in automotive aerodynamics* (No. 2004-01-1308). SAE Technical Paper.
- [14]. Schlichting, H., and Gersten, K. (2017). *Fundamentals of Boundary-Layer Theory*. In *Boundary-Layer Theory* (pp. 29-49). Springer, Berlin, Heidelberg.
- [15]. Katz, J., and Plotkin, A. (1991). *Low-Speed Aerodynamics – From Wing Theory to Panel Models*. Int. edn.
- [16]. Drela, M., and Giles, M. B. (1987). *Viscous-inviscid analysis of transonic and low Reynolds number airfoils*. *AIAA journal*, 25(10), 1347-1355.
- [17]. Wauquiez, C. (2009). *Shape optimization of low speed airfoils using Matlab and Automatic Differentiation*. VDM Publishing.

APPENDICES

```

Side 1 free transition at x/c = 0.4731 51
Side 2 free transition at x/c = 0.8657 68
idif Ue xi dudx      1 0.20956977      2.41899490E-03 86.635063
Uenew xinew         2 4.26534191E-02 4.92334366E-04

 1 rms: 0.1500E+00 max: -.9691E+00 T at 51 1 RLX: 0.516
  a = 1.000 CL = 0.5833
  Cm = -0.1031 CD = 0.00619 => Cdf = 0.00510 CDp = 0.00110

Side 1 free transition at x/c = 0.4902 52
Side 2 free transition at x/c = 0.8690 69

 2 rms: 0.1022E+00 max: -.8385E+00 C at 52 1 RLX: 0.596
  a = 1.000 CL = 0.5787
  Cm = -0.1020 CD = 0.00567 => Cdf = 0.00484 CDp = 0.00082

Side 1 free transition at x/c = 0.5497 55
Side 2 free transition at x/c = 0.8867 70

 3 rms: 0.4563E-01 max: -.7656E+00 C at 55 1 RLX: 0.653
  a = 1.000 CL = 0.5775
  Cm = -0.1017 CD = 0.00576 => Cdf = 0.00431 CDp = 0.00145

SETBL: Xtr??? n1 n2: 8.2391243 8.9999952
Side 1 free transition at x/c = 0.5497 55
Side 2 free transition at x/c = 0.8886 70

 4 rms: 0.8582E-01 max: -.1997E+01 C at 55 1 RLX: 0.250
  a = 1.000 CL = 0.5769
  Cm = -0.1015 CD = 0.00584 => Cdf = 0.00432 CDp = 0.00152

Side 1 free transition at x/c = 0.5553 56
Side 2 free transition at x/c = 0.8890 71

 5 rms: 0.1912E-01 max: 0.2616E+00 D at 56 1
  a = 1.000 CL = 0.5741
  Cm = -0.1010 CD = 0.00590 => Cdf = 0.00432 CDp = 0.00158

Side 1 free transition at x/c = 0.5676 56
Side 2 free transition at x/c = 0.8885 70

 6 rms: 0.8798E-02 max: 0.1862E+00 C at 56 1
  a = 1.000 CL = 0.5736
  Cm = -0.1009 CD = 0.00594 => Cdf = 0.00421 CDp = 0.00173

Side 1 free transition at x/c = 0.5631 56
Side 2 free transition at x/c = 0.8878 70

 7 rms: 0.3083E-03 max: -.4960E-02 C at 56 1
  a = 1.000 CL = 0.5736
  Cm = -0.1009 CD = 0.00595 => Cdf = 0.00424 CDp = 0.00171

Side 1 free transition at x/c = 0.5632 56
Side 2 free transition at x/c = 0.8878 70

 8 rms: 0.3067E-05 max: -.5555E-04 C at 70 2
  a = 1.000 CL = 0.5736
  Cm = -0.1009 CD = 0.00595 => Cdf = 0.00424 CDp = 0.00171
plradd ia,ip,cpol      1      83 0.24060994

Point added to stored polar 1
Point written to save file original_xfoil_result.txt
Point written to dump file ref_orig.txt

```

Figure 1. Iteration process for original Xfoil's solution

```

Side 1 free transition at x/c = 0.4907 104
Side 2 free transition at x/c = 0.8744 174

 1 rms: 0.2133E+00 max: -.1747E+01 T at 104 1 RLX: 0.286
  a = 1.000 CL = 0.5655
  Cm = -0.0959 CD = 0.00605 => Cdf = 0.00514 CDp = 0.00092

Side 1 free transition at x/c = 0.4957 104
Side 2 free transition at x/c = 0.8549 170

 2 rms: 0.2266E+00 max: -.2993E+01 T at 104 1 RLX: 0.167
  a = 1.000 CL = 0.5617
  Cm = -0.0955 CD = 0.00767 => Cdf = 0.00526 CDp = 0.00242

MRCHDU: Convergence failed at 108 side 1 Res = 0.5553E+01
Side 1 free transition at x/c = 0.5023 106
Side 2 free transition at x/c = 0.8549 170

 3 rms: 0.1308E+00 max: -.1534E+01 T at 107 1 RLX: 0.326
  a = 1.000 CL = 0.5421
  Cm = -0.0914 CD = 0.00551 => Cdf = 0.00487 CDp = 0.00064

Side 1 free transition at x/c = 0.5099 107
Side 2 free transition at x/c = 0.8389 167

 4 rms: 0.8656E-01 max: -.1400E+01 T at 107 1 RLX: 0.357
  a = 1.000 CL = 0.5358
  Cm = -0.0900 CD = 0.00637 => Cdf = 0.00494 CDp = 0.00142

MRCHDU: Convergence failed at 109 side 1 Res = 0.9353E+00
Side 1 free transition at x/c = 0.5242 110
Side 2 free transition at x/c = 0.8376 167

 5 rms: 0.1669E+00 max: -.3487E+01 C at 110 1 RLX: 0.143
  a = 1.000 CL = 0.5384
  Cm = -0.0907 CD = 0.00558 => Cdf = 0.00459 CDp = 0.00099

Side 1 free transition at x/c = 0.5256 110
Side 2 free transition at x/c = 0.8404 167

 6 rms: 0.7087E-01 max: -.1030E+01 T at 110 1 RLX: 0.486
  a = 1.000 CL = 0.5334
  Cm = -0.0894 CD = 0.00592 => Cdf = 0.00471 CDp = 0.00122

Side 1 free transition at x/c = 0.5487 115
Side 2 free transition at x/c = 0.8403 167

 7 rms: 0.9264E-01 max: -.1863E+01 C at 115 1 RLX: 0.268
  a = 1.000 CL = 0.5367
  Cm = -0.0901 CD = 0.00574 => Cdf = 0.00444 CDp = 0.00130

```

Figure 2. Iteration process for adapted Xfoil's solution

```

Side 1 free transition at x/c = 0.5512 115
Side 2 free transition at x/c = 0.8444 168

 8  rms: 0.3394E-01  max: -.4322E+00  T at 115 1
    a = 1.000      CL = 0.5339
    Cm = -0.0894   CD = 0.00592 => Cdf = 0.00447  CDp = 0.00145

Side 1 free transition at x/c = 0.6033 126
Side 2 free transition at x/c = 0.8452 168

 9  rms: 0.8350E-01  max: 0.1500E+01  C at 126 1  RLX: 0.937
    a = 1.000      CL = 0.5325
    Cm = -0.0893   CD = 0.00627 => Cdf = 0.00419  CDp = 0.00208

Side 1 free transition at x/c = 0.5818 121
Side 2 free transition at x/c = 0.8423 168

10  rms: 0.2797E-01  max: 0.3081E+00  D at 125 1
    a = 1.000      CL = 0.5384
    Cm = -0.0904   CD = 0.00579 => Cdf = 0.00426  CDp = 0.00153

Side 1 free transition at x/c = 0.5779 121
Side 2 free transition at x/c = 0.8501 169

11  rms: 0.5258E-02  max: 0.1070E+00  C at 121 1
    a = 1.000      CL = 0.5375
    Cm = -0.0902   CD = 0.00586 => Cdf = 0.00421  CDp = 0.00164

Side 1 free transition at x/c = 0.5766 120
Side 2 free transition at x/c = 0.8495 169

12  rms: 0.5170E-03  max: -.1029E-01  D at 125 1
    a = 1.000      CL = 0.5376
    Cm = -0.0902   CD = 0.00585 => Cdf = 0.00422  CDp = 0.00163

Side 1 free transition at x/c = 0.5763 120
Side 2 free transition at x/c = 0.8496 169

13  rms: 0.1196E-04  max: -.1747E-03  C at 120 1
    a = 1.000      CL = 0.5376
    Cm = -0.0902   CD = 0.00585 => Cdf = 0.00423  CDp = 0.00163
plradd ia,ip,cpol      1      203 0.22437604

Point added to stored polar 1
Point written to save file adapted_xfoil_result.txt
Point written to dump file ref_adap.txt

```

Figure 2. Iteration process for original Xfoil's solution (cont.)